**POLITEHNICA UNIVERSITY
OF BUCHAREST**

**Doctoral School of Electronics, Telecommunications
and Information Technology**

Decision No. 831 from 15-04-2022

Ph.D. THESIS
SUMMARY

Amer Abbood Osman AL-BEHADILI

CARACTERIZAREA MATERIALELOR SOLIDE ȘI
LICHIDE PE BAZĂ DE SENSORI MICROSTRIP DE
SENSIBILITATE MARE
CHARACTERIZING BOTH SOLID AND LIQUID
MATERIALS BASED ON HIGH SENSITIVITY
MICROSTRIP SENSORS

THESIS COMMITTEE

Prof. Dr. Ing. Gheorghe BREZEANU Politehnica Univ. of Bucharest	President
Prof. Dr. Ing. Teodor PETRESCU Politehnica Univ. of Bucharest	PhD Supervisor
Prof. Dr. Ing. Tudor Petru PALADE Univ. Tehnică din Cluj-Napoca	Referee
Prof. Dr. Ing. Ioan NICOLAESCU Academia Tehnică Militară	Referee
Conf. Dr. Ing. Iulia Andreea MOCANU Politehnica Univ. of Bucharest	Referee

BUCHAREST 2023
_____

Acknowledgements

Firstly, I might want to thank Prof. Dr. Eng. Teodor Mihai PETRESCU my PhD supervisor. For three years my supervisor supports me in all trends to develop my skills in the microwave engineering field. I really appreciate his patience and his guidance to extract my best in this field. The commutation of ideas between us was very productive.My proposed subject has been studied and investigated with my supervisor. A lot of cases related to microwave engineering field has been discussed and refined to step up thesis level. I am happy and satisfied with our results.

Secondly, I might want to thank Dr. Eng. Iulia MOCANU in the Faculty of Electronics, Telecommunications and Information Technology at University Politehnica of Bucharest for helping to overcome many difficulties, such as fabricating and measuring the proposed structures in the thesis, in addition to publishing in journals with high impact factor. She is really deserves all appreciation.

Alot thanks to Prof. Dr. Ing. George LOJEWSKI and Conf. Dr. Ing. Nicolae MILITARU for their advice and support inorder to direct the thesis in best form.

I might want to say my honest thankfulness to Romanian people, from whom I have seen nothing but the best, whether they are in Politehnica University or elsewhere. Finally, I say my deepest gratitude to my family.

Content

Chapter 1

Introduction

This doctoral thesis will study dielectric constant measurements based on microwave sensors which are created by microstrip structures. Over the last few years, accurate measurement of material properties has been a major concern. There is a growing requirement for wireless sensing for various fields such as physicists, chemists, military applications, mission-critical industrial, biologists [1] and structural health monitoring [2][3].

In general, the microwave techniques there are two types of material property characterization methods: non-resonant techniques, which are based on microwave propagation, as well as resonant techniques that are based on microwave resonance. Non-resonant approaches are used to provide comprehensive information on electromagnetic characteristics across a large frequency range, whereas resonant techniques are used to obtain accurate information on dielectric properties at a single frequency or many discrete frequencies. Non-resonant and resonant techniques are frequently used to achieve precise knowledge of material properties by altering the complete information obtained from non-resonant and resonant techniques over a specific frequency range [4].

1.1 Non-Resonant Sensing Methods in survey literature

Signal reflection and transmission/reflection measurements are the main components of non-resonant sensing systems. The material properties are extracted in a reflection measurement based on the signal reflection from the sample due to the discontinuity of the impedance introduced by the sample inside a transmission line construction. The material characteristics are extracted by a transmission/reflection measurement based on the signal reflected from the sample, the signal transmitted through the sample, and the relevant scattering equations associating the scattering parameters of the section of transmission line loaded with sample material.

1.1.1 Transmission/Reflection method

A measurement using the Transmission/Reflection method involves placing a sample of material under test, MUT in a transmission line segment and measuring complicated scattering characteristics, S-parameters of the two-port with a vector network analyzer, VNA. Measurement of reflected, S_{11} and transmitted, S_{21} signals is part of the approach.

1.1.2 Reflection method (The open ended coaxial probe)

In this technique, the material characterization is measured by pressing it to the flat face of a solid material or by flooding the probe into a liquid. The reflection coefficient S_{11} will be measured using a vector network analyzer, and an appropriate analytical model for sample-loading of the probe's aperture will be used to determine the permittivity [5].

1.1.3 Free space method

The free space technique allows materials to be measured at high temperatures or in hostile situations. The approach works across a wide frequency range, and the measurement requires a large, flat material sample. Two antennas (transmitting and receiving) are normally mounted facing each other and connected to a network analyzer.

1.2 Resonant Sensing Methods in survey literature

Resonant techniques are utilized describe the properties of a material with high precise and sensitivity in comparison with non-resonant techniques. Resonant methods are generally based on the change in resonator properties (which are resonant frequency and quality factor) due to the perturbation the electromagnetic fields of the resonator's with the specimen under test, commonly called the "cavity perturbation technique" [4].

Quasi-static electrically tiny resonators are utilized in this technique; they are generally made with a loop and a gap splitting the loop into two sections. The circulating current in the loop induces inductance, and the gap between the loops causes an effective capacitance to build across it, resulting in an electrically tiny structure that echoes. There are many types of resonant structures available are proposed for characterization of the electric properties of materials as in [6].

In order to summarize the above, Table1.1 shows a general review of different measurement techniques and conversion methods, as well as their advantages and disadvantages [7]–[9]. The main focus of the thesis is on resonant methods and their conversion methods for extracting dielectric properties of materials in terms of complex permittivity.

Table. 1.1 *Comparisons of the most common strategies [10].*

Measurement Techniques	Advantages	Disadvantages	Materials Under Test	Conversion Methods	Speed	Accuracy
Transmission and reflection	- Used to measure samples with medium to high loss - Used to determine both permittivity and permeability	- Limitation of measurement accuracy of the air-gap effects - Low accuracy for a sample whose length is a multiple of one-half-wavelength in the materials	- Solid - Liquid - Sheet surface	- NRW - NIST iterative - New non-iterative	Fast Slow Fast	Medium Good Good
Open-ended coaxial probe	- Easy sample preparation - Measurement for the large number of samples in a short time after the calibration - Measurement can be performed in a temperature-controlled environment	- Supports only reflection measurement - Affected by the air-gap for measurement in the specimen	- Liquids - Biological specimens - Semi-solids	RFM	Fast	Good
Free space	- Suitable for high-frequency measurement - Allows non-destructive measurement - Measures material under test in hostile conditions - Evaluates both permittivity and permeability properties	- Needs large and flat material under test - Multiple reflections between the surface of the sample and the antenna - Diffraction effects at the edge of the sample	- High temperature materials - Large flat solid - Gas - Hot liquid	- NIST iterative - New non iterative - NRW	Slow Fast Fast	Good Good Medium
Resonant methods	- Suitable to measure small samples -Both the sample and cavity are analysed using approximate expression	- Requires Vector Network Analyser (VNA) - Exclusive for narrow frequency bands	- Rod shaped solid materials - Gas - Liquids	- Frequency - quality factors - S-paramter	Slow	Good

1.3   Presentation of the field of the doctoral thesis

Modern developments in the field of microwave planar sensors have produce to a renovated interest in biological, industrial, medical, and chemical applications that are qualified of performing real-time measurement of properties of material. The evolution of high-sensitivity microwave planar sensors is desired for highly precies complex permittivity measurements to observe the small changes among various material specimens. Therefore, the field of this thesis is to study, analysis, design, and fabricate modern microwave planar sensors and further challenges of their sensitivity and selectivity. Moreover, the techniques of the complex permittivity extraction (real and imaginary parts) were discussed based on the different approaches of mathematical models. The results of this thesis may simplify improvements of and an alternative solution for the enhancement of microwave planar sensors' normalized sensitivity for material characterization.

1.4   The Scope of the doctoral thesis

The objective of this thesis is focus on resonant methods and their conversion methods which are based on microstrip planar sensors for extracting dielectric properties of materials in terms of complex permittivity (Real part and imaginary part). In this thesis, three new models of microstrip planer sensors for solid and liquid materials characterization have been investigated. Two of three models have been fabricated, and tested. while third model has been simulated only to reason of manufacture limitation. One of These models also aim to estimate the hydration of human body through urine testing in addition to complex permittivity of the tested urine. several mathmatical expression models have been obtained by each sensor in ordere to compute the sample complex permittivity with high accuracy.

The main objects of this thesis are:

- design and demonstrate highly sensitive microsrtip resonator structure based sensors for different sensing applications.

- intent to design the structure based on available FR-4 substrate that can be easily fabricated on a single metal layer.

- simplifying the production process by testing sample in the simplest method instead of complexity such as having etched a microfluid channel, etc.

- The investigate of complex permittivity should be carried out through full-wave electromagnetic simulator, mathematical model and measurments.

- publishing the results in high impact factors journals.

1.5   Content of the doctoral thesis

After reviewing shown in chapter 1 concerning various studies and examples of implementation of microwave planar sensors in material characterization. Chapter 2 is reviewing the mathematical models for complex permittivity extraction and recent developments and their outlook directions. This chapter is mainly focused the techniques of the complex permittivity extraction on microwave sensor-based planar resonators for material properties' extraction such as solids, and liquids binary mixtures. The most prominent techniques which based on resonant methods and their transform methods in order to excerpting the materials complex permittivity are: Polynomial Curve Fitting Model, The Least Squares Model Based on Peak Attenuation, The Least Squares Model Based on the Quality Factor, Debye Relaxation Equation, and Machine Learning Methods.

In chapter 3, a new approach for extracting electrical parameters of the equivalent circuit of complimentary split ring resonators (CSRRs) loaded transmission line, based on the frequency band where negative electrical permittivity occurs, is proposed. For this reason CSRR coupled to microstrip transmission line has been proposed and the behavior of the frequency band where negative permittivity appears is investigated, in order to specify the fundamental frequencies that are needed to calculate the electrical parameters of equivalent circuit. The procedure provides the electrical characteristics of CSRR (inductance, L_c, capacitance, C_c and intrinsic resonant frequencies). The obtained equivalent circuit model of CSRR loaded transmission line has been simulated and a good agreement is achieved between the results derived from the simulation and the ones form the equivalent circuit model. Further validity of the proposed approach was confirmed by applying different lengths of transmission line (host line). Nevertheless, the results of minimum insertion loss which were determined by the provided equivalent circuit model are remaining compatible with the simulation. All investigation results in this chapter are done depending on Ansoft HFSS simulator and Matlab.

In chapter 4, a new model of microwave planar sensor established on the complementary split ring resonator (CSRR) as well as an air hole in substrate of the structure is introduced for a precise measurement of materials permittivity. The CSRR structure with hole was selected for the sensitivity analysis, the results obtained show high sensitive compared with CSRR structure without hole. The sensor in the form of CSRRs operating at a 1.74–3.4 GHz band was explained. The proposed sensor resonant frequency was shifted from 3.4 to 1.74 GHz according to the change of sample permittivity from 1 to 10. A numerical model was provided of the proposed sensor to determine the real permittivity of MUT in terms of the measured resonant frequency. It is found that the proposed sensor provides sensitivity between 1.2-2.5 times greater than sensitivity of conventional planer sensors have the same relative permittivity of the substrate (without hole).While, proposed sensor sensitivity reach to

3 times greater than conventional planer sensors have low loss Rogers substrate (without hole).

In chapter 5, a sensor using modified Split Ring Resonators (SRRs) is designed, simulated, fabricated, and used for advanced investigation and precise measurements of the real part and imaginary part solid dielectrics' permittivity. Adding vertical strips tightly coupled to the outer ring of the SRR leads to the appearance of two resonant frequencies at 1.24 GHz and 2.08 GHz. This modified geometry also assures an improved sensitivity. Using the full wave electromagnetic solver, both the unloaded and loaded sensors are investigated. The numerical simulations are used to develop a mathematical model based on a curve fitting tool (Origin bro) for both resonant frequencies, allowing obtaining analytical relations for real and imaginary parts of permittivity as a function of the sample's thickness and quality factor. The sensor is designed and fabricated on 1.6 mm thick FR-4 substrate. The measurements of different samples, such as transparent glass, acrylic glass, plexiglass, and Teflon, confirm that the modified SRR sensor is easy to implement and gives accurate results for all cases, with measurement errors smaller than 4.5%. In addition, the measurements highlight the importance of the second resonant frequency in the cases in which numerical limitations do not allow the usage of the first resonant frequency (1 mm thick sample).

In chapter 6, a microstrip highly sensitive differential sensor for complex permittivity characterization of urine samples is designed, fabricated, and tested. The sensing area contains open-stub resonators, and the working frequency of the unloaded sensor is 1.25 GHz. The sensor is easily implemented on an affordable substrate FR-4 Epoxy with a thickness of 1.6 mm. A Teflon beaker is attached to the sensor without affecting the measurements. Different ratios of water-urine mixtures have been considered for measurement. Different samples of water content in urine were tested with percentages, such as 0% urine (100% water), 20% urine, 33% urine, 50% urine, 66% urine and 100% urine. The complex permittivity as well as ratio of water content for the samples has been determined based on a mathematical model and the results of the measurements. The sensitivity of the sensor is around 3 %.

Chapter 2

Techniques of Complex Permittevity Extraction

The focus of this thesis is on microwave sensor-based planar resonators for extracting material properties such as solids, liquids, and binary mixtures. Material properties such as the permeability and conductivity of materials are not included. While, the material properties in terms of the complex permittivity (real and imaginary parts) is extracted.

2.1 Extraction of Complex Permittivity Using Mathematical Modeling

To measure a material's dielectric properties, it's usually necessary to know the suitable measurement technique and conversion methods. In chapter 1, Table1.1 shows a comprehensive overview of different measurement techniques and conversion methods, as well as their advantages and disadvantages.

The main focus of this thesis is on resonant methods and their conversion methods for extracting materials' dielectric properties in terms of complex permittivity.

2.1.1 Polynomial Curve Fitting Model

The resonance frequency is subjected on the relative permittivity of experimented materials [11].When the sensor is loaded with the material, a numerical model is needed to characterize the permittivity of the tested materials based on recorded factors such resonance frequency change and insertion loss. The material permittivity equation is recovered from the measured scattering data using the curve fitting technique, and the sample permittivity is mathematically represented in terms of the curve fitting technique, such as linear or polynomial.

2.1.2   The Least Squares Model Based on Peak Attenuation

In order to construct a mathematical sensing model for the sensor, the resonance frequency and peak attenuation, which are connected to complex permittivity (real and imaginary parts), are required established on a binary mixture of aqueous solutions [12]. To determine the attributes of the tested mixture of liquid materials in terms of the complex permittivity ($\varepsilon' + j\varepsilon''$), the binary mixture measurements are first used for calibration. To achieve this, a mathematical relation based on shifting frequency and peak attenuation in relation to the complex permittivity of the investigated binary mixture materials (such as water–ethanol and water–methanol solutions) will be applied.

2.1.3   The Least Squares Model Based on the Quality Factor

The complex permittivity is affected by both the resonance frequency and the sample quality factor, as stated in [13].The slight fluctuation in permittivity with regard to the change of the resonance frequency and the Q-factor is represented using a simplified model. The difference between the Q-factor when the sensor is loaded with the tested sample and the reference Q-factor, which can be generated in a matrix [14], is defined as the change of the Q-factor (ΔQ).

2.1.4   Debye Relaxation Equation

Polar liquids will be pierced by the microwave sensor's electric field, which will cause the molecule to rotate and lose energy. In terms of resonance frequency and quality factor, the response of the developed sensor will be altered. The real and imaginary parts of the complex permittivity of the test polar liquids are revealed by these behaviors. The complex permittivity of polar liquids can be written as $\varepsilon = \varepsilon'(\omega)\text{-}j\varepsilon''(\omega)$, where the real and imaginary parts of the complex permittivity are defined by the Debye theory. In the literature, the Debye relaxation model for DI water may be found [14].

2.1.5   Machine Learning Methods

More research should be done to look at mathematical modeling based on machine learning methodologies for quickly and accurately analyzing observed data. Because of their strong learning ability and excellent accuracy, mathematical techniques based on Neural Networks (NNs) have recently been used for complex permittivity extraction [15].

Chapter 3

Novel Method to Extract the Equivalent Circuit of Complementary Split-Ring Resonator Unit Cell (CSRR)

In this chapter the all scattering parameters of CSRR loaded transmission line are identified by using specific frequency band interval where negative permittivity occurs, in order to be utilized in extraction of equivalent circuit.

3.1 Description of the Technique

At resonance, CSRRs have small electrical dimensions and hence the unit cell can be depicted by agency of lumped-element equivalent circuits. The technique explains that the effect of negative permittivity band has an essential role to extracting the equivalent circuit model of a CSRR-loaded transmission line.

The inductance and capacitance of the host microstrip line, L and C are computed as the per-unit-cell inductance and capacitance of the host transmission line [16] (pp. 24–27), while the computation of L_c and C_c will explained further on. The frequency $f_z = \frac{1}{2\pi\sqrt{L_c(C+C_c)}}$ can be determined through full wave electromagnetic simulation directly, or it can be extracted as representing the mid-point of the interval of negative permittivity band ($f_z = f_s + (f_o - f_s)/2$) as depict in Figure 3.1, as well as the frequency f_z, locate at (Re ε <0 and the phase $\neq \pi/2$). This is considered an advantage given by the characteristic of negative permittivity band.
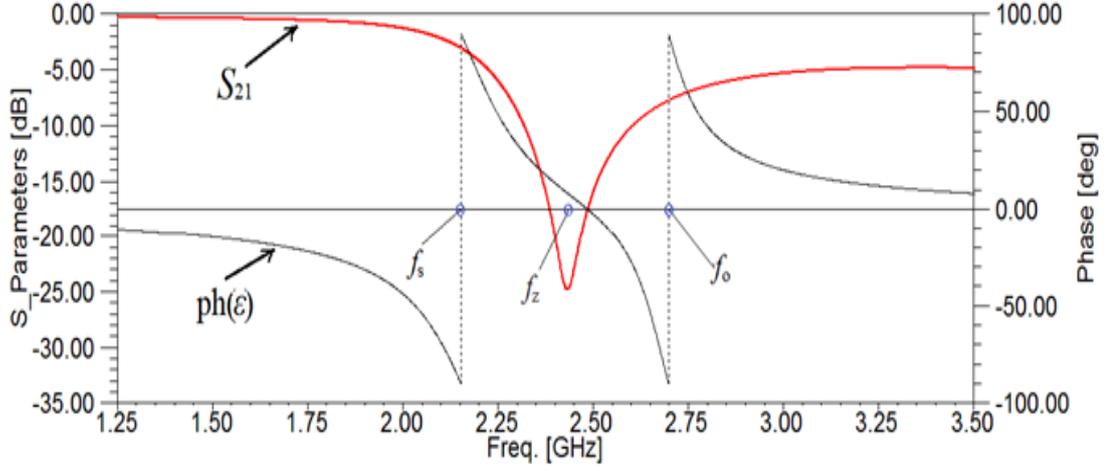
Figure 3.1. *Permittivity phase response and magnitude of transmission zero frequency (S_{21}) of CSRR unit cell.*

The expression for f_z dependents on two parameters (L_c, C_c) which are not yet calculated, therefore an additional condition is need.

The transmission matrices of the unit cell can be written [17] (pp.177-193).

$$\begin{bmatrix} Z_{11} & Z_{12} \\ Z_{21} & Z_{22} \end{bmatrix} = \begin{bmatrix} \dfrac{j\omega X_L}{2} + \dfrac{C(1-\omega^2 L_c C_c)}{1-\omega^2(C+C_c)L_c} & \dfrac{C(1-\omega^2 L_c C_c)}{1-\omega^2(C+C_c)L_c} \\ \dfrac{C(1-\omega^2 L_c C_c)}{1-\omega^2(C+C_c)L_c} & \dfrac{j\omega X_L}{2} + \dfrac{C(1-\omega^2 L_c C_c)}{1-\omega^2(C+C_c)L_c} \end{bmatrix}, \tag{3.1}$$

$$\begin{bmatrix} A & B \\ C & D \end{bmatrix} = \begin{bmatrix} \dfrac{Z_{11}}{Z_{21}} & \dfrac{Z_{11}Z_{22}-Z_{12}Z_{21}}{Z_{21}} \\ \dfrac{1}{Z_{21}} & \dfrac{Z_{22}}{Z_{21}} \end{bmatrix}, \tag{3.2}$$

The dispersion relation of CSRR unit cell can be calculated as [94].

$$\cos(\beta\ell) = \frac{A+D}{2} = 1 + \cfrac{1}{2\left(\cfrac{L_c}{1-\cfrac{\omega^2}{\omega_0^2}-\cfrac{1}{C\omega^2}}\right)}. \tag{3.3}$$

where ω is the angular frequency where the phase is π/2 (lower frequency, f_s).

The frequency f_o is obtained directly as the upper frequency at which Re ε=0 and the phase is equal to π/2. Therefore, it is not required a representation of reflection coefficient (S_{11}) curve on Smith Chart to find f_o as in traditional method [18]. This is the second advantage offered by features of negative permittivity band.

10

Now, from f_z, f_s, f_o and expression (3.5), the parallel impedance (L_c, C_c) can be determined. In order to demonstrate the authenticity of the proposed technique, the procedure described above is used to obtain electrical parameters of the CSRR unit cell which is designed and simulated and the results are synthesized in Table 3.1.

Table 3.1 Extracted parameters of the structure.

Lumped elements	L (nH)	C (pF)	C_c (pF)	L_c (nH)
values	2.667	0.6727	1.0625	2.4661

From the elements in Table 3.1, zero transmission in frequency response of the structure can be obtained by electrical simulation (using MATLAB) as well as electromagnetic simulation as depicted in Figure 3.2. Good agreement has been achieved between electrical simulation and electromagnetic one, which validates the structure model and the proposed procedure for parameter extraction.
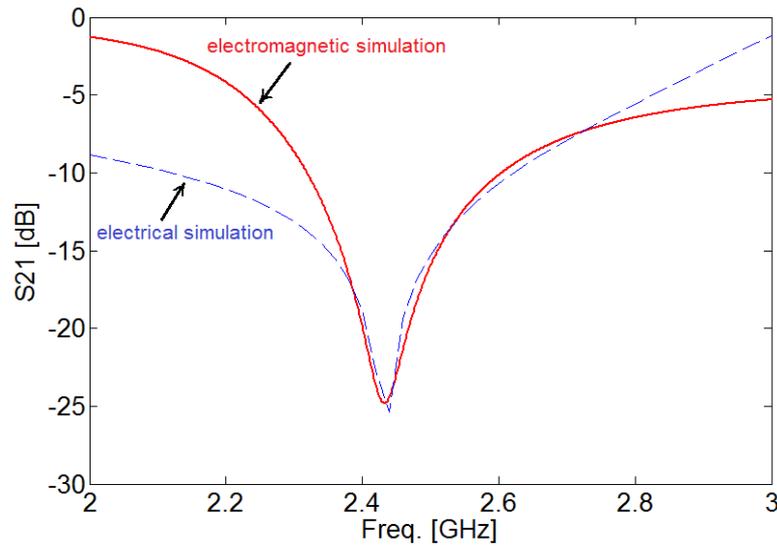
Figure 3.2 Magnitude of the transmission coefficient with respect to the frequency for the structure.

Name	Freq	Ang	Mag	RX
■ m1	2.6130	24.1509	0.9126	0.9991 + 4.4608i
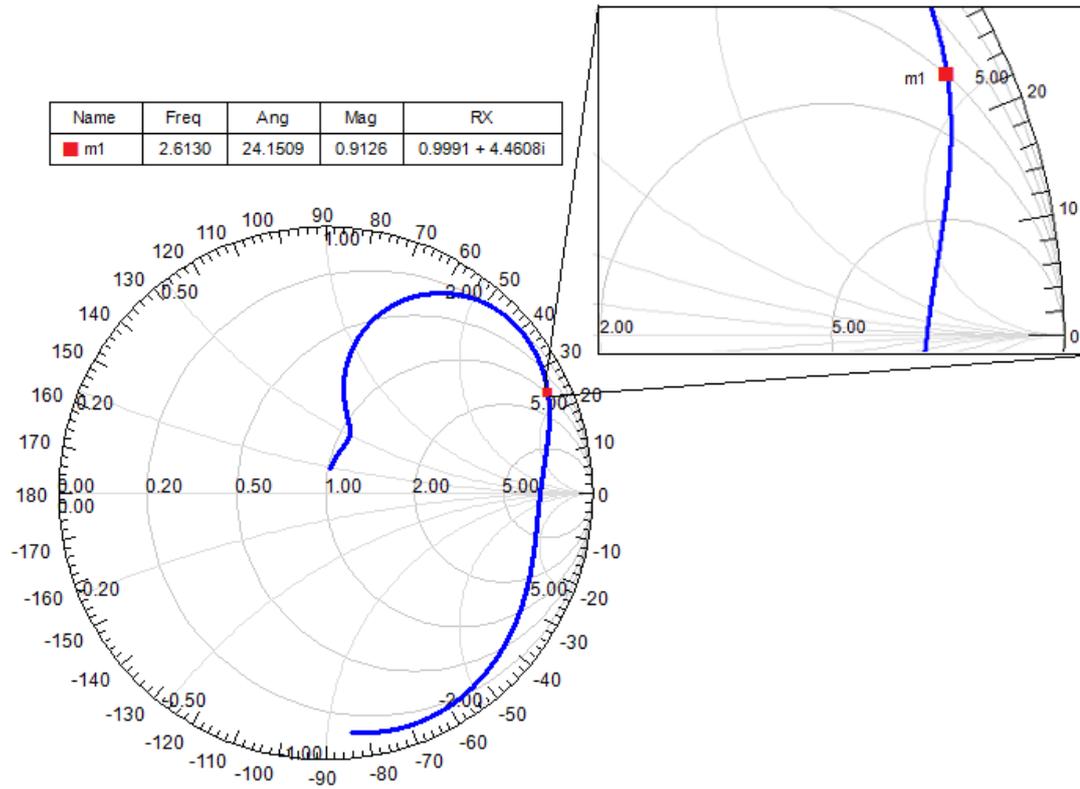
Figure 3.3 *Electromagnetic simulated of reflection coefficient (S_{11}) for the CSRR unit cell on a Smith Chart*.

Further investigation is shown in Figure 3.3, which depicts the electromagnetic simulation of the reflection coefficient (S_{11}) on Smith Chart. It can be noted that the intersection of S_{11} curve with unit resistance circle provides finding f_o (2.613 GHz) (as in traditional method), in agreement with f_o (2.65 GHz). Hence, further confirm of the validity of the proposed procedure is obtained.

Chapter 4

Complimentary split ring resonator sensor with high sensitivity based on material characterization

4.1 Design and analysis of the structure

A new model of microwave planar sensor established on the complementary split ring resonator (CSRR) as well as an air hole in substrate of the structure is introduced for a precise measurement of materials permittivity. The proposed structure is one type of the quasi-static consist of substrate with hole and split rings in two ports in which an inductance stimulated by circulating current in the rings and the effective capacitance increased across the gap between the rings, hence electrically small resonator is achieved. To detail the performance of the proposed structure, a comparison must be made with traditional structure and verify the results of each structure. The configurations of two substrates of CSRR unit cells without and with hole are shown in Figures 4.1 (a) and 3.1(b), respectively.
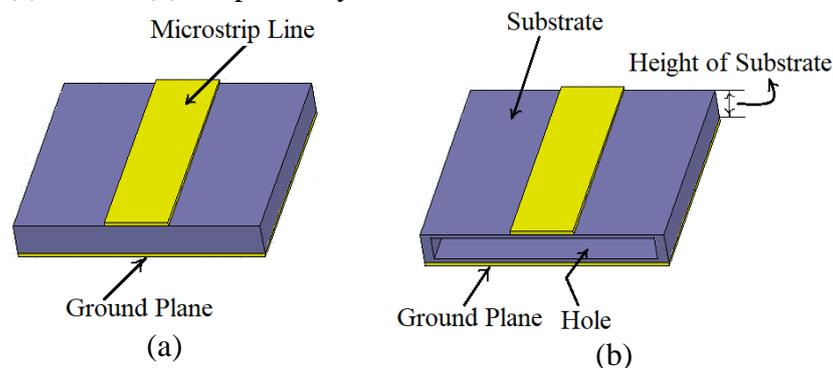

Figure 4.1 *Layout structure of substrate of CSRR unit cell: (a) without hole (traditional layout), (b) With hole.*

4.2 Comparison and Analysis Sensitivity of CSRR Unit Cell with and without Hole

For a fair comparison between the proposed structure and traditional CSRR unit cell, the unit cell areas as well as the design parameters in Figure 4.1 (b) are taken as identical throughout this discussion. Initially both structures are modeled and the simulation is carried out to achieve the scattering parameter (S_{21}) in the band of specified frequency.

The per-unit-cell inductance and capacitance (L, C) which related to the type of permittivity of the structure (at air hole) are obtained, while L_c and C_c of both structures are calculated by [19].The calculated lumped parameters are depicted in Table 4.1.

Table 4.1 Lumped parameters extracted for both structures.

Lumped Parameters	Traditional CSRR unit Cell	Proposed Structure
L (nH)	3	2.76
C (pF)	0.67	0.4
C_c (pF)	1.28	2
L_c (nH)	2.255	0.97

It is important to note from Table 4.1 that the value of L_c related with the proposed structure is much smaller than in traditional CSRR unit cell, at the same time it can be observed L_c is the most affected parameter due to presence of the hole as compared with other parameters. This basically means that as expression (4.1), the resonant frequency of the proposed structure will be vastly higher than the traditional structure. This can also be explained by the fact that the resonant frequency of such resonators actually increase with decreasing value of permittivity of structure.

After calculating the equivalent circuit's parameters, it results the sensitivity analysis which is represented by varying the medium and is depicted in Figure 4.2.
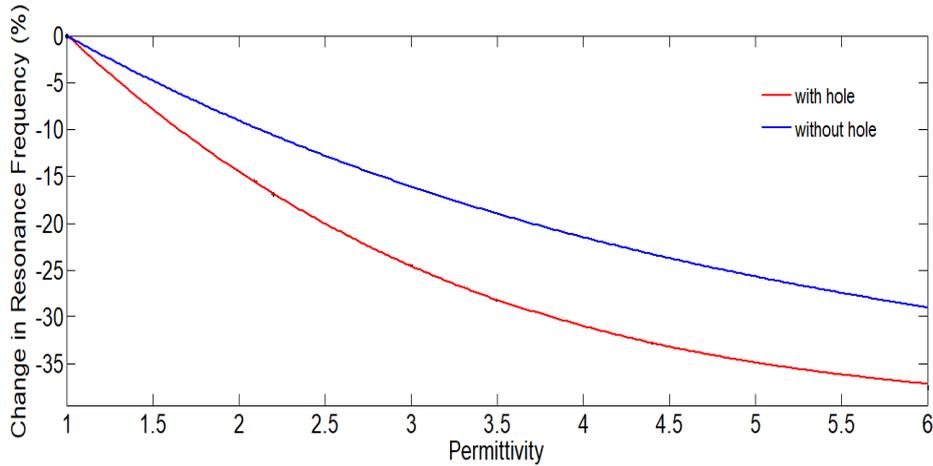
Figure 4.2 *Behaviors of the Proposed structure and CSRR unit cell for permittivity changes in the surrounding medium. The relative f_r shift is calculated with respect to the reference f_r when the medium is vacuum.*

From Figure 4.2 it can be concluded that the proposed structure is more sensitive to change in permittivity compared with traditional structure. However for further evaluation, the two structures will be used to establish two models as planar sensors to be analyzed moreover for the purpose of permittivity characterization.

4.3   Deciding the Sensor Model

Due to the change in the permittivity of the material under test (MUT), the capacitance of CSRR will change hence a shifting in resonance frequency is obtained (the inductance of the CSRR is considered to be unchanged in case of dielectric materials). In this paper, two proposed structures (one with hole as shown in Figure 4.8 and the other without hole) having equal unit cell area, are investigated for the sensitivity analysis, and detailed verification is presented in next sections.

The proposed sensor in Figure 4.3 has (24mm×30mm) external cross section area, with folded microstrip line in order to make the hole in the substrate as low as possible while keeping the orientation of open ends perpendicular to the excitation of magnetic field. All remaining design parameters will be the same that in Figure 4.2.
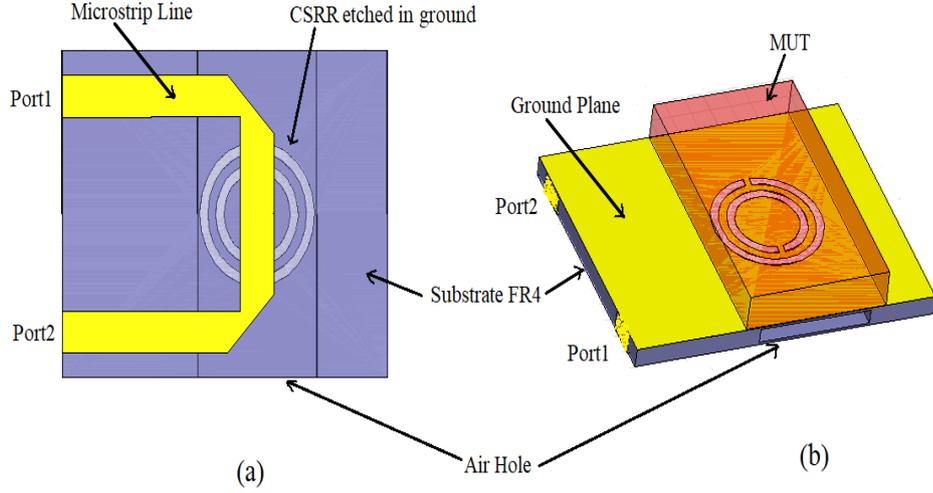
Figure 4.3 *Layout of proposed planer sensor: (a) Top view with transparent substrate, (b) Sight view of the structure with MUT put over ground plane.*

4.4 Deposition of Sample Permittivity

The effect of loading the sensor with MUT is observed in terms of the resonant frequency of the proposed sensor as discussed previously. The inverse square of the resonant frequencies, extracted from the simulated transmission coefficient data, the inverse square of resonant frequencies, extracted from the simulated transmission coefficient data are both plotted with the corresponding permittivity of MUT as shown in Figure 4.4. It can be seen the fluctuation of f_h^{-2} and f_r^{-2} with ε_{MUT} is linear.

As indicated in section 4, the region of the sensor which loaded by MUT has capacitance proportional to the permittivity of MUT and hence, the inverse square of the resonant frequency is directly proportional to the MUT permittivity (as spotted in (4.1). Therefore in order to integrate all the above data, the permittivity of MUT is mathematically represented as follow:

$$\varepsilon_{\text{MUT}} = -118.9\left(f_h^{-2}\right)^3 + 87.14\left(f_h^{-2}\right)^2 + 17.9 f_h^{-2} - 1.176. \qquad (4.1)$$

Expression (4.1) is obtained using the curve fitting tool, which provides a numerical model of the proposed sensor to determine the real permittivity of MUT in terms of the measured resonant frequency.
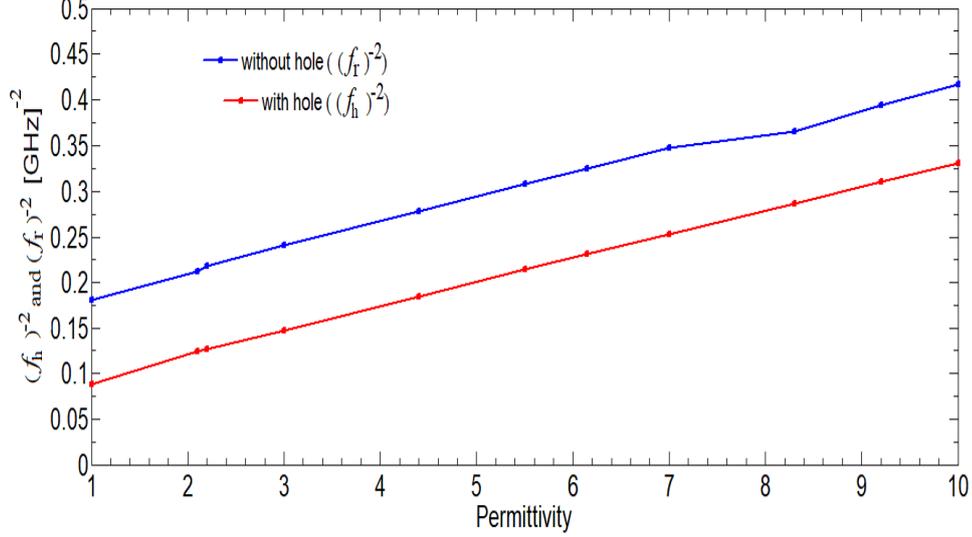
16

Figure 4.4 *Reprezentation of the inverse squared resonant frequencies for the sensors with hole and without hole*

4.5 Comparison results of CSRR planar sensors with and without hole

After standardization, a number of materials are described using the proposed sensors. Resonant frequencies of S_{21} data for all conditions are recorded using HFSS. The simulated results are also compared with the criterion data obtainable in the reference [20] which are given in columns 2 of Table 4.2. Moreover the sensitivity of the sensor has been calculated and the results are listed in Table 4.2.

The sensitivity in resonance-based dielectric sensors is defined as:

$$S(\%) = \frac{f_{\varepsilon_r} - f_{ref}}{f_{ref} \cdot (\varepsilon'_r - 1)}. \tag{4.2}$$

From Table 4.2 it can be concluded that the proposed sensor with hole in substrate presents frequency shift values greater than in conventional sensors. Hence the proposed sensor provides sensitivity between 1.2-2.5 times greater than sensitivity of conventional planer sensors have the same relative permittivity of the substrate (without hole). While, proposed sensor sensitivity reach to 3 times greater than conventional planer sensors have low loss Rogers substrate (without hole) [20].

***Table 4.2** Simulated results of variation resonant frequencies using proposed CSRR and conventional CSRR based planer sensor techniques.*

Technique ⟶ Materials ↓	Reference values of the sample [115]	Δf_r (Air-MUT) [GHz]	S (%)	Proposed sensor based CSRR without hole. [GHz]	Δf_r (Air-MUT) [GHz]	S (%)	Proposed sensor based CSRR with hole. [GHz]	Δf_r (Air-MUT) [GHz]	S (%)
Air(ε_r=1,tanδ=0)	f_r =1.15	0	---	f_r=2.35	0	---	f_r=3.42	0	---
Teflon(ε_r=2.1,tanδ=0.001)	f_r =1.095	0.055	4.6	f_r=2.173	0.177	7.4	f_r =2.844	0.576	18.4
RO3003(ε_r=3,tanδ=0.0013)	f_r =1.05	0.1	4.7	f_r =1.897	0.453	11.9	f_r =2.612	0.808	15.5
FR4(ε_r=4.4,tanδ=0.02)	f_r =0.95	0.2	6.4	f_r=1.695	0.655	11.3	f_r=2.33	1.09	13.7
Max. frequency shift when ε_r change from 1 to 10	37.5%	---		34%	---		47.2%	---	
Structure cross section (cm x cm)	10 x 5	---		2.4 x 3	---		2.4 x 3	---	

Chapter 5

Modified Split Ring Resonators Sensor for Accurate Complex Permittivity Measurements of Solid Dielectrics

5.1   Modified SRR Sensor Design

5.1.1   Resonant Structures for Higher Selectivity

In this chapter, a sensor using modified Split Ring Resonators (SRRs) is designed, simulated, fabricated, and used for advanced investigation and precise measurements of the real part and imaginary part solid dielectrics' permittivity. The SRR structure consists of two highly closed concentric metallic split ring resonators etched on a substrate, with two gaps orientated in opposite directions, as shown in Figure 5.1(a). When a magnetic field perpendicular to the ring surface is applied, a current is induced through the rings. These currents go from one ring to another due to the distributed capacitance that appears between them [21].

5.1.2   Resonant Frequencies Analysis

The material under test (transparent box) is placed on the SRR unit cells of the VS-SRR sensor, as depicted in Figure 5.1(a), covering the whole area of the sensor for having an efficient perturbation of the E-field and assuring the resonance frequency shift required for precise measurements. When the resonance occurs, the total electric field will be confined to a smaller region of split ring resonator, where the sample is usually placed as shown. This confined electric field is capable of sensing an even smaller change in the dielectric constant of the test sample.

The response of the microwave sensor to the change in the effective dielectric constant of the surrounding can be noticed in terms of the change in resonant frequency and the quality factor of the loaded structure [22]. The intensity of the electric field through the sensor, analyzed at the two resonant frequencies, is presented in Figure 5.4(b).
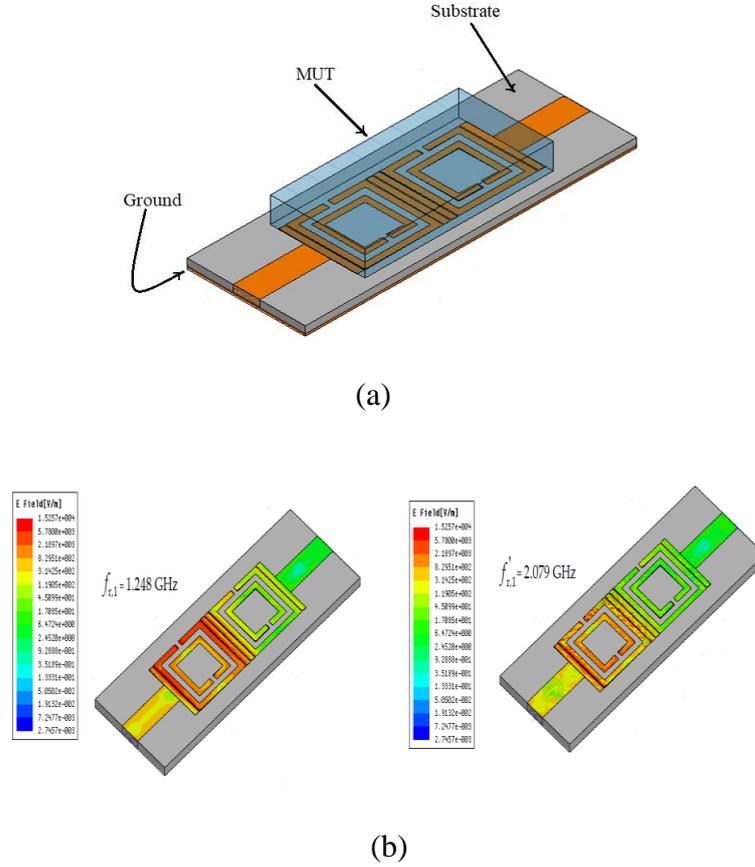

(a)

(b)

Figure 5.1 The vertical strips (VS)-SRR sensor: (a) Setup of the VS-SRR sensor with material under test (MUT) placed over the two modified SRR unit cells, (b) 3D representation of the intensity of the electric field at the first resonant frequency and at the second resonant frequency.

5.1.3 Deduction of the Real Part of the Permittivity

To determine the type of dependency between the resonant frequency and the real part of the permittivity, we consider the expression for the resonant frequency depending on the quality factor [23].

$$Q = \frac{f_r}{2\pi\sqrt{L(C+C_{\text{load}})}}. \tag{5.1}$$

The capacitance introduced by the load, Cload depends directly proportional to the real part of the electrical permittivity [23], so considering relation (4.1) as well,

we obtain the resonant frequency. So, for the proposed sensor, the affected transmission coefficient due to sample loading can be observed in Figure 5.2.

The inverse squares of the resonant frequencies ($f_{r,1}$ and $f'_{r,1}$) are extracted from the simulated transmission coefficient data and the results with the corresponding real permittivity (ε'_r) of the MUT are plotted and showed in Figures 5.2 (a) and (b).
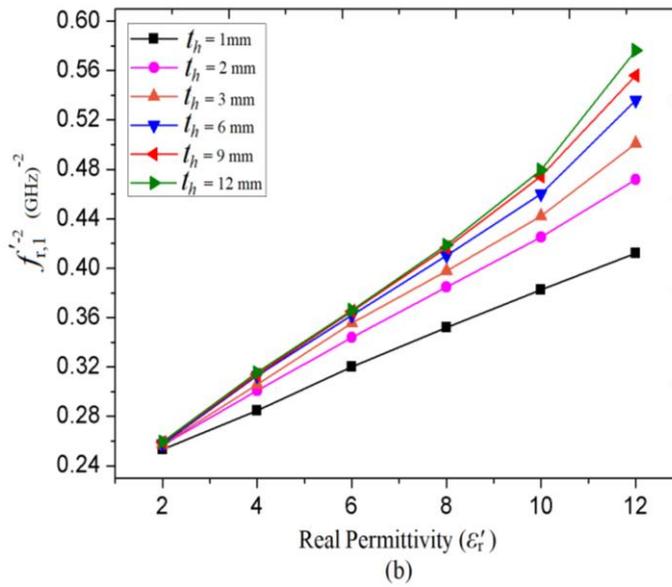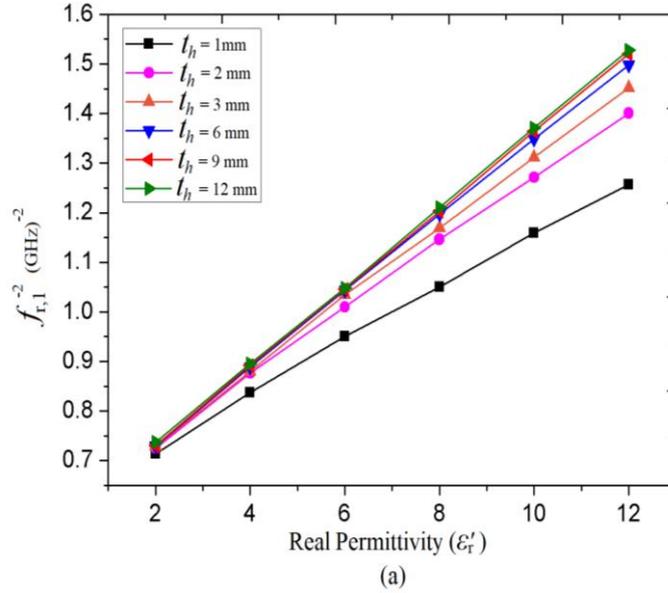

(a)

(b)

Figure 5.2. *Resonant frequencies in terms of real permittivity (ε'_r) for different thickness of MUT. (a)First resonant frequency $(f_{r,1})^{-2}$, (b) second resonant frequency $(f'_{r,1})^{-2}$*

In order to combine all the above effect, the dielectric constant of the specimen is mathematically expressed in terms of the family of straight lines as well as a family of exponential curves, where the freelance parameters are the resonant frequencies ($f_{r,1}$ and $f'_{r,1}$ expressed directly in GHz) and the sample thickness (t_h expressed directly in mm). By taking this aspect into consideration when using the fitting tool practically, the accuracy of the numerical model increases. So, based on the plotted data and using the curve fitting tool, we obtain the expressions for the real permittivity as a function of the MUT's thickness and the two resonant frequencies.

$$\varepsilon'_r = \frac{1}{1.88 \cdot 10^{-4} \cdot \ln(18472.96 \cdot \ln(t_h))} \cdot \ln\left[\frac{39.6824 - (f_{r,1})^{-2}}{39.095}\right], \tag{5.2}$$

$$\varepsilon'_r = \exp\left\{2.2607 \cdot \ln\left[\frac{(f_{r,1})^{-2} - 5.373}{\frac{0.2336}{t_h + 0.1266} - 1.2}\right]\right\}. \tag{5.3}$$

5.1.4 Deduction of the Imaginary Part of the Permittivity

The relation between the loss tangent, $\tan\delta$, the quality of the proposed sensor after loading the MUT, Q_{MUT}, the real part of the permittivity, ε'_r, and the imaginary part of the permittivity, ε''_r is given by [24].

$$Q_{MUT} = \frac{1}{\tan\delta} = \frac{\varepsilon'_r}{\varepsilon''_r}. \tag{5.4}$$

where Q_{MUT} states the quality factor of the proposed sensor after loading the MUT, which may be determined applying relation (5.4). The imaginary part of the complex permittivity is therefore obtained using (5.2) and (5.4). The quality factor is extracted from the simulation result of S_{21} as depicted earlier in Figure 5.2, for each resonance frequency. After that, the inverse of the quality factors for each corresponding loss tangent are plotted in Figure 5.2 (a), (b).

As in the previous case of the real part of permittivity, a commercially available software Origin Pro 8 is used to determine the numerical model for both extracted results in Figure 5.2 (a) and (b) as presented in expressions (5.5) and (5.6), respectively.

$$\tan\delta = \exp\{0.687 \cdot \ln[8.165 \cdot 10^{-3} \cdot (36.812 \cdot \varepsilon'^{-0.338}_r - Q_{MUT})]\}, \tag{5.5}$$

$$\tan\delta = 0.1574 \cdot \ln\left[\frac{Q^{-1}_{MUT} + 0.0023}{0.04503 - 0.0318 \cdot (0.94427)^{\varepsilon''_r}}\right]. \tag{5.6}$$

After determining the ε'_r from (5.2), (5.3) and tanδ from (5.5), (5.6) the imaginary part of the complex permittivity can be obtained using (5.4).
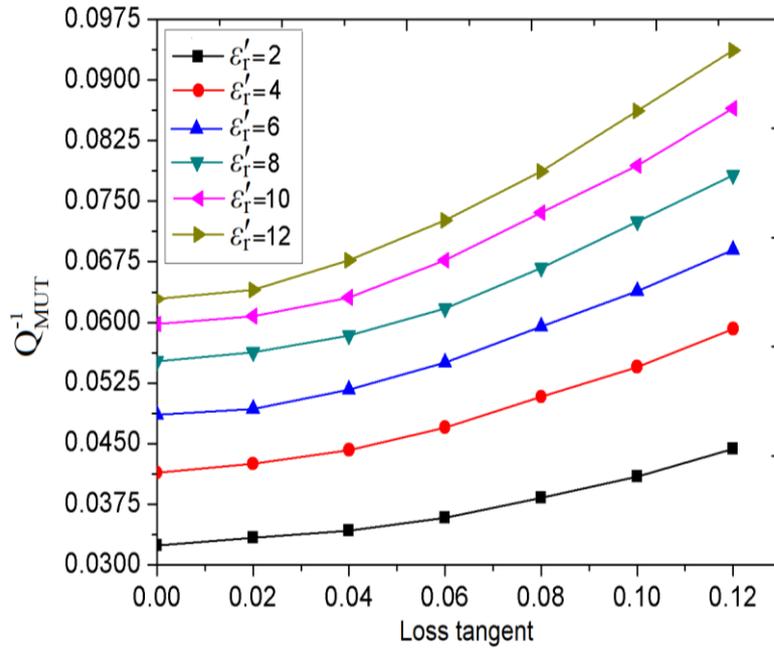
(a)
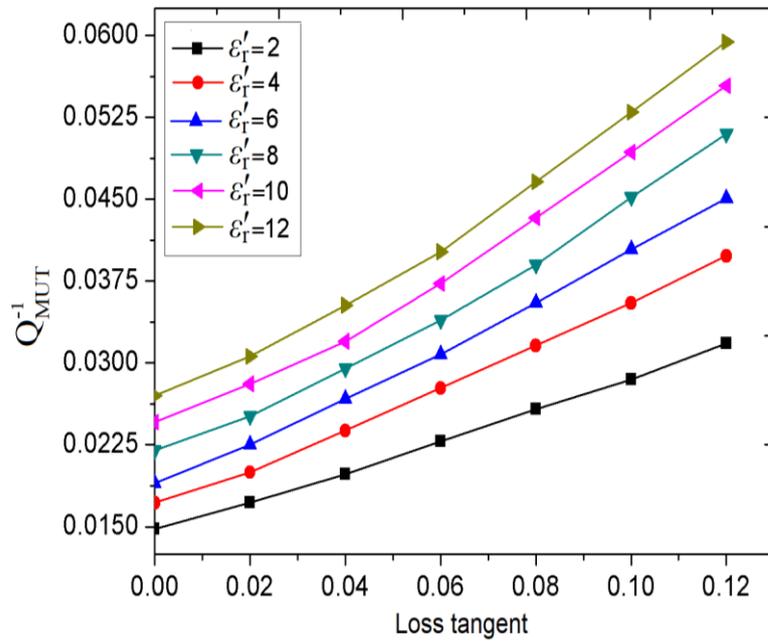
(b)

Figure 5.3. *Inverse of Q-factor in terms of tanδ for various values of ε'_r, depending on resonant frequency: (a) $f_{r,1}$, (b) $f'_{r,1}$*

5.2 Results

The sensor proposed in Figure 5.1 is now implemented and measured. The substrate used is FR-4 (relative permittivity ε_r = 4.4 and the dissipation factor, tanδ, is approximately 0.02), with a thickness of 1.6 mm and cooper metallization electrodeposited on both sides of the substrate, with a thickness of 18 µm.

(a)

(b)
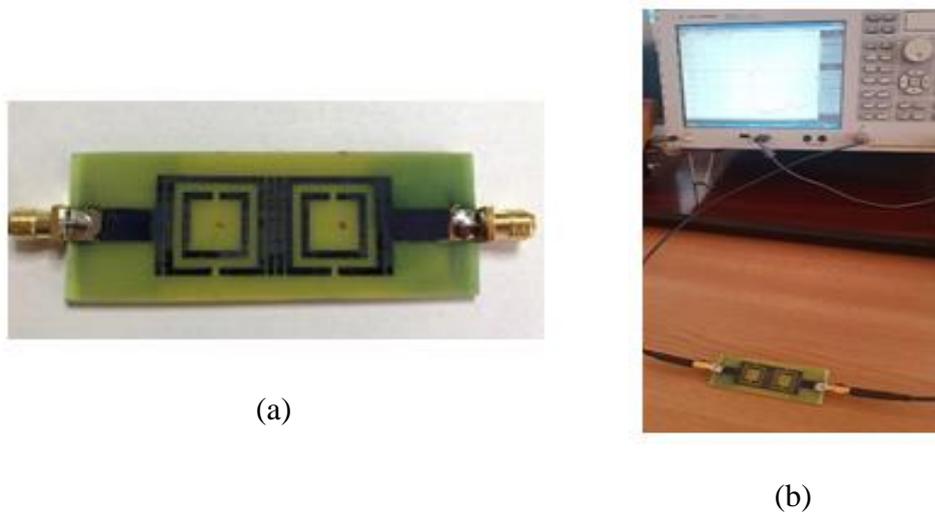
Figure 5.4 *Implementation of the sensor: (a) the sensor implemented on a FR-4 substrate, with 1.6 mm, with Cooper metallization on both sides, (b) measurement setup.*

Both resonant frequencies obtained after measurement for different types of MUT are considered and using relations (5.2) and (5.3), two possible values for the real part of the permittivity are obtained. They are compared with reference values [24]-[26] and the results, including errors, are synthesized in Table 5.2.

Table 5.2 *Real part of the complex permittivity for different materials under test.*

Material	t_h [mm]	ε'_r	f_{r1} [GHz]	ε'_{r1}	error [%]	f_{r2} [GHz]	ε'_{r2}	error [%]
Transparent Glass	5	6	0.9856	5.872	2.12	1.671	6.163	2.72
Acrylic Glass	5	2.7	1.127	2.647	1.93	1.902	2.629	2.59
Acrylic Glass	2	2.7	1.139	2.644	2.04	1.924	2.627	2.7
Teflon	10	2.1	1.152	2.125	1.19	1.941	2.017	3.91
Plexiglas	1	2.597	1.155	-	-	1.97	2.512	3.24

For the measurement of the imaginary part of permittivity, first, the measured quality factor Q_{MUT} is replaced in relations (5.5) and (5.6) and the value of the loss tangent, tan δ is obtained. It is compared to the reference values [24]-[26] and the results are given in Table 5.3.

Table 5.3 *Loss tangent for different materials under test.*

Material	t_h [mm]	tan δ	Q_{MUT1}	$tanδ_1$	error [%]	Q_{MUT2}	$tanδ_2$	error [%]
Transparent Glass	5	0.005	20.18	0.00512	2.39	47.39	0.0051	3.26
Acrylic Glass	5	0.02	26.12	0.019417	2.92	56.1	0.0203	1.88
Acrylic Glass	2	0.02	26.07	0.020532	2.66	56.05	0.0205	2.7
Teflon	10	0.0003	28.5317	0.000308	2.75	69.335	0.0003085	3.24
Plexiglas	1	0.0008	26.648	-	-	65.43	0.00082	3.12

Next, using relation (5.4), the imaginary part of the permittivity is determined. The results of the measurements are given in Table 5.4.

Table 5.4 *Imaginary part of the complex permittivity for different samples.*

Material	t_h [mm]	ε_r''	ε_{r1}''	error [%]	ε_{r2}''	error [%]
Transparent Glass	5	0.03	0.030065	0.215467	0.031431	4.497
Acrylic Glass	5	0.054	0.051397	4.82074	0.053369	1.169
Acrylic Glass	2	0.054	0.054287	0.530756	0.053854	0.27129
Teflon	10	0.00063	0.000655	3.8888	0.00062	1.231
Plexiglas	1	0.002078	-	-	0.00206	0.8548

The results in the two tables show that the sensor can be used successfully to accurately characterize the dielectric parameters (dielectric constant and loss tangent) for both low-losses and lossy dielectrics, as well as for high dielectric constants dielectrics and small dielectric constants dielectrics.

Chapter 6

Differential Microstrip Sensor for Complex Permittivity Characterization of Organic Fluid Mixture

Water balance in the human body is a key indicator for good functioning of different metabolic activities [27]. In particular, the hydration state of a person is influencing the blood pressure, the heart rate, body temperature, etc. so, it is very important to have accurate measurements about this state. The hydration assessment techniques for the body involve urinary, hematologic, whole-body, and sensory measurements [28]. Determining the level of hydration when analyzing urine is one of the most efficient, easy, and least invasive methods, so sensors capable of doing this have been investigated often.

6.1 Sensor's layout

After considering the resonant structures best suited for our application, the next step is to design the whole sensor. It will be a differential one, consisting of two identical Wilkinson power dividers and two pairs of microstrip transmission lines, each of them loaded with two open stub resonators as designed in the previous subchapter. Also, a beaker made of Teflon is perfectly attached to the surface of the two open stub resonators not to have air between the beaker and the sensor. The beaker is filled with liquids that will be considered samples under test (SUT). The layout of the sensor is given in Figure 6.1.
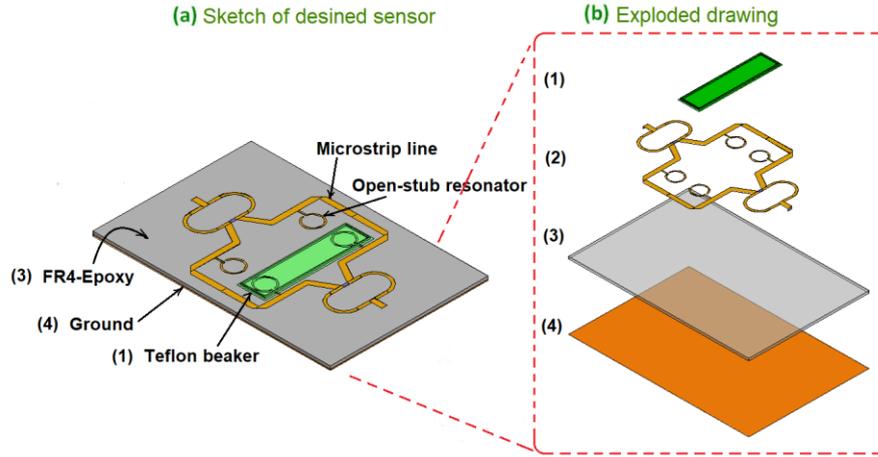
(a) Sketch of desined sensor

(b) Exploded drawing

Microstrip line
Open-stub resonator
(3) FR4-Epoxy
(4) Ground
(1) Teflon beaker

(1)
(2)
(3)
(4)

Figure 6.1. *The layout of the sensor, including an exploded view drawing of each layer.*

From Figure 6.1, the Teflon beaker is located on the proposed sensor's top surface, covering one pair of open stub resonators. To make sure that the beaker does not affect the sensor's performance, a simulation of S_{21} parameter was carried in HFSS for two cases: the sensor without and with a beaker on top.

By loading the sensor with liquids under test (LUT) in the beaker, the symmetry is broken, and another resonant frequency appears. The reference will be considered the case when the sensor is loaded with pure water. This behavior will be proven by the results of both simulations and measurements for different organic mixtures in the next sections.

Next, liquid mixtures of water and urine in different percentages are used to simulate the sensor's frequency behavior. The percentage of fresh water content in the mixture is varied from 0% (100% urine) to 100% (0% urine) with a step of 3.226% (0.025163 mL) giving 32 data groups of the simulated results. The values for the relative permittivity for water and for urine are 50 and 81, respectively and for conductivity are 0.01S/m and 1.75 S/m, respectively [29].

The simulation results for the transmission characteristic of the sensor for some of the cases is given in Figure 6.2 (a). All cases are considered for further analytical computations and for determining the quality factor, the resonance frequency and conductivity, in Figure 6.2 (b), (c), (d). The quality factor was determined using relation (6.1) and the data provided by simulation for the insertion loss and conductivity.
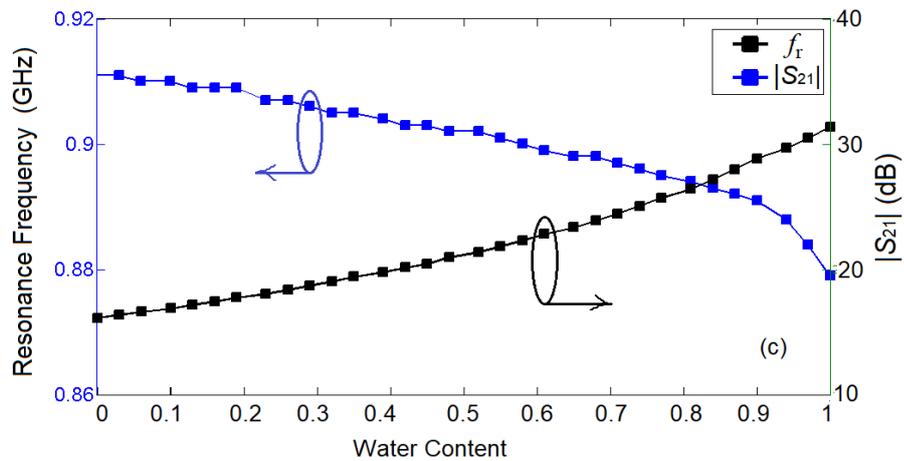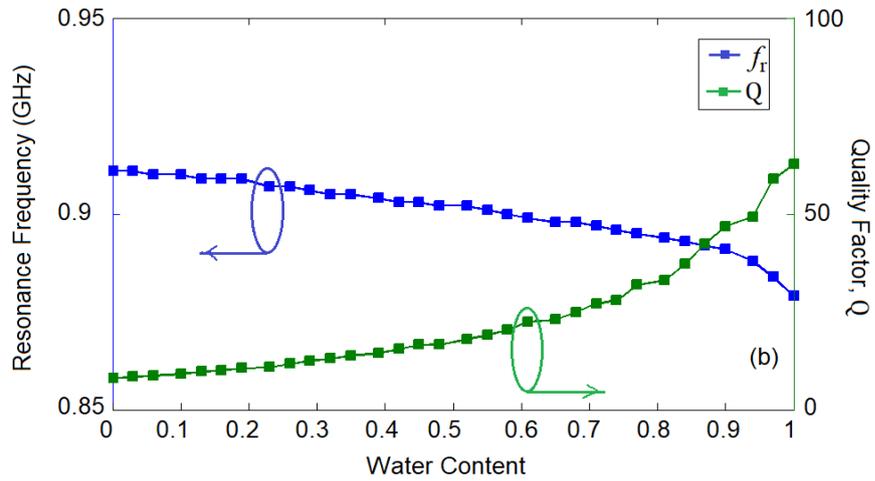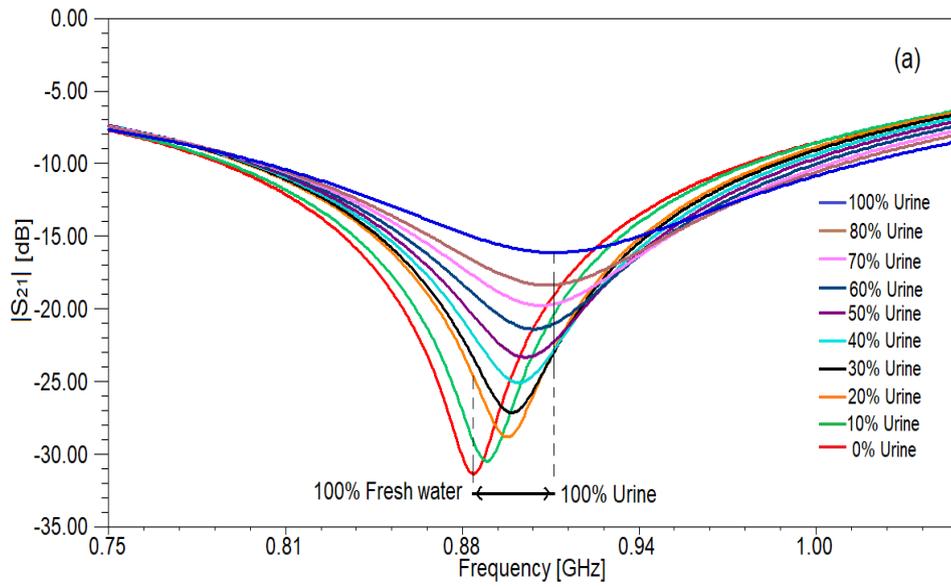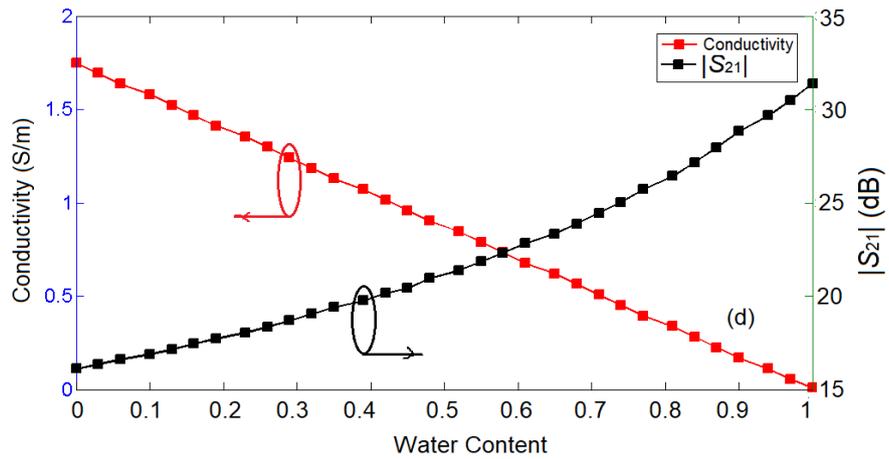
Figure 6.2 *a) Insertion loss for 10 ratios of water-urine mixture; b) Quality factor and resonance frequency for 32 ratios of water-urine mixture, c) Insertion loss and resonance frequency for 32 ratios of water-urine mixture; d) Conductivity and insertion loss for 32 ratios of water-urine mixture.*

6.2 Results

The sensor proposed in Figure 6.1 is now implemented and measured. The substrate used is FR-4 (relative permittivity ε_r = 4.4 and the dissipation factor, tan δ, is approximately 0.02), with a thickness of 1.6 mm and cooper metallization electrodeposited on both sides of the substrate, with a thickness of 18 μm.

Figure 6.3 *Photograph of the fabricated sensor for measuring different urine samples.*

A set of samples under test is selected and used for measurements. Practically, healthy male morninig urine is combined with fresh water in different ratios and 6 samples are obtained as explained in Table 6.1 and depicted in Figure 6.4.

Table 6.1 *Urine-water mixture samples.*

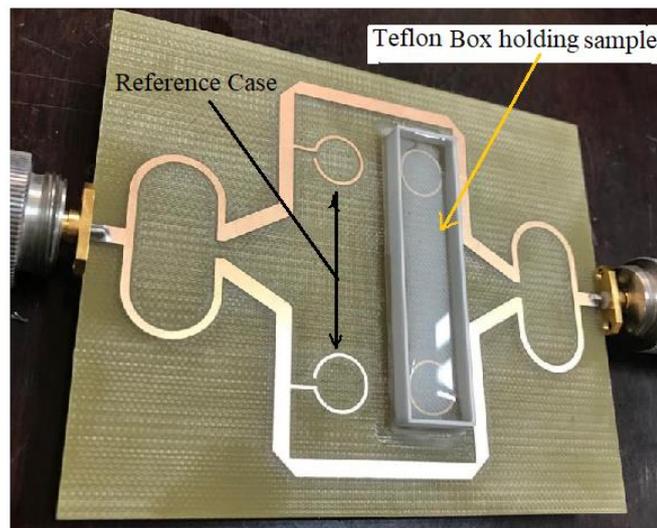| Sample	Water (%)	Urine (%)
1	100	0
2	80	20
3	66	33
4	50	50
5	33	66
6	0	100

Figure 6.4   *Different ratios urine-water mixtures used for measurements.*

For each measurement, the sensor is placed on a rough, stable surface and the SUT is carefully placed to cover the whole sensing area, making sure no pellicular effect exists. To reduce the effect of impurities and of humidity from the previous test sample, the beaker is washed thoroughly, then rinsed with water and dried by cotton brush. Finally, the next urine sample is dropped in the beaker. Then, using the Agilent E5071C network analyzer, the magnitude of S_{21} parameter is measured. The results of the measurements are given in Figure 6.5.
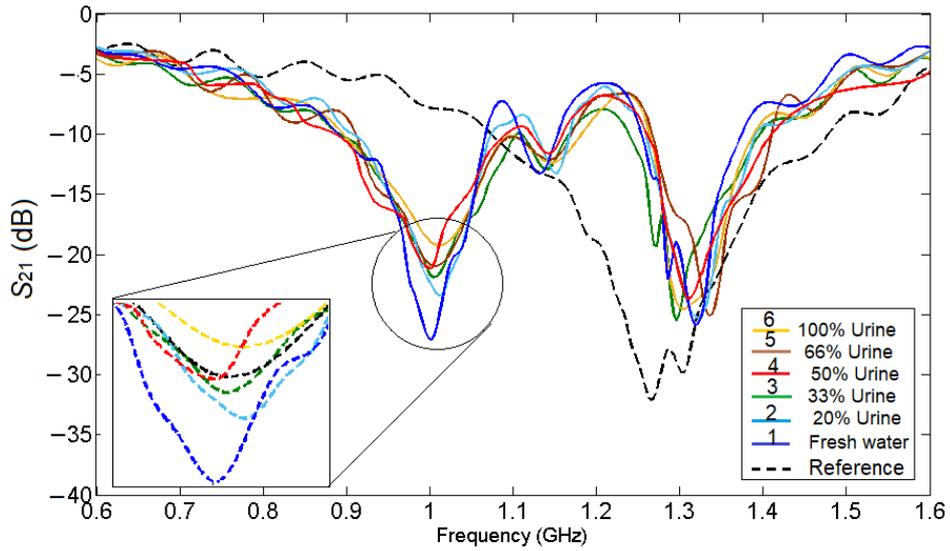
Figure 6.5 *Measurement results for the samples presented in Figure 6.4, where the reference is represented by the unloaded sensor.*

Analyzing the results in Figure 6.5, it can be seen that the differential behavior of the sensor, meaning when it is not loaded, only one resonant frequency appears and once mixtures are added into the beaker, the symmetry is broken, and two resonant frequencies appear.

The real and imaginary part of the complex permittivity for the different urine-water mixtures in Table 6.1 are depicted in Figure 6.6. Indeed, urine–water mixture is not a binary mixture such as ethanol–water, methanol–water, etc. Nevertheless, a good assent with the forecast presented by the Weiner model that extracted relying on simulation results. Evidence the validity of the proposed sensor to determine the reasonable complex permittivity of urine-water mixture. The computed values of real and imaginary parts are added to Table 6.2.
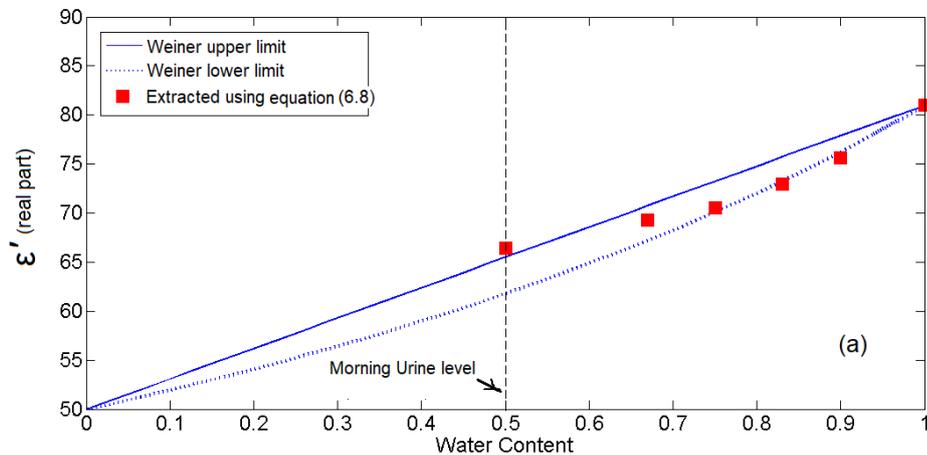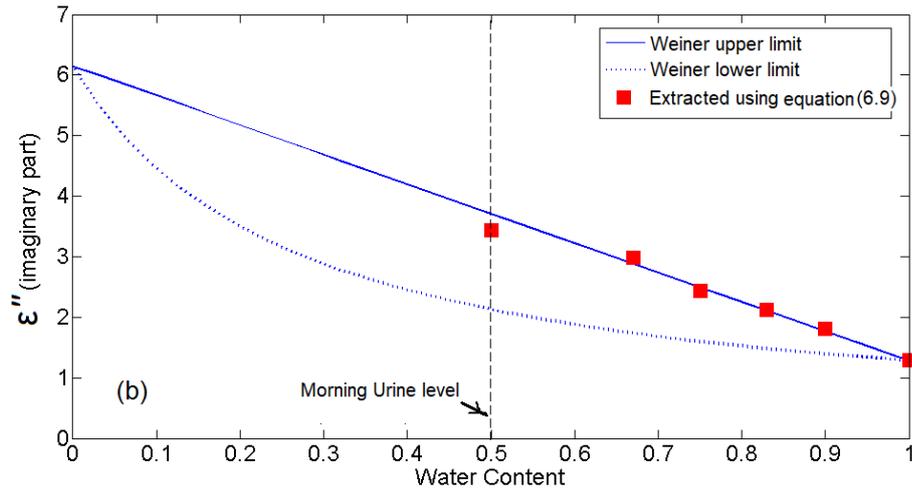
Figure 6.6 *Both the real (a) and the imaginary (b) parts of the permittivity in mixtures of urine/water.*

Table 6.2 *Measurement results.*

Sample	S_{21} [dB]	Quality factor	$\Delta\sigma$ (S/m)	$\Delta|S_{21}|$ [dB]	ε'_r	ε''_r	Water [%]	S (%)
1	-26.93	34	-	-				
2	-23.39	23.181	0.348	3.54	75.6161	1.8058	80	2.53
3	-21.87	21.659	0.4986	5.06	72.9279	2.1292	71	2.71
4	-21.1	20.632	0.5744	5.83	69.3282	2.4418	67	2.84
5	-20.96	16.839	0.5882	5.97	69.3282	2.98054	66	2.826
6	-19.32	14.1456	0.7498	7.61	66.4429	3.4337	57	2.89

6.3 Discussion

In Table 6.3, the results for the sensitivity are compared to the ones in literature. Note that there few investigations regarding measurements of mixtures between water and organic liquids, such as urine. Still, the references in Table 6.3 refer to sensors measuring liquid mixtures with high relative permittivity.

Urine is a complex compound made of inorganic and organic compounds. All of them influence the electrical permittivity, so it is very important to have accurate sensors to determine these parameters.

When compared to other resonance-based microwave microfluidic sensors, it can be observed that the relative permittivity is in a narrower range, from 66 to 74.

Additionally, the proposed sensor is not a microfluidic one but still has some ad-vantages when compared to them. The main advantages refer to the fact that the tech-nological process is much simplified as no microfluidic channels are required, just a Teflon beaker attached to the sensor, which does not influence the frequency behavior of the sensor. Thus, the sensor proposed in this paper can be used successfully to detect with great sensitivity the changes in the values of the complex permittivity of urine samples. This can be used to determine metabolic changes and help diagnose different disorders.

Table 6.3 *Comparison between various resonance-based microwave microfluidic sensors.*

Sensor	Type of fluid	Central frequency [GHz]	ε'_r range	S (%)	Ref.
Substrate integrated waveguide	Isopropanol	3.6	4-76	0.15	[30]
CSRR	Ethanol	2.37	9-79	0.03	[31]
Shunt-connected series LC resonator	Ethanol	2	30-80	0.44	[32]
CSRR	Ethanol	1.6	30-80	0.626	[33]
Open CSRR	Methanol	0.9	35-80	1.8	[34]
CSRR	Urine	4	-	-	[35]
Dumbbell-Shaped Defect Ground Structures	Isopropanol	1.05	75–80	1.02	[36]
CSRR	Ethanol	1.618	9–79	0.626	[37]
RLC	Glycerol	2.3	8.22–79.5	2.117	[38]
Open SRR	Isopropanol	1.8	75–80	1.6	[39]
Classic	Glycerol/Ethanol	1.9	-	1.316	[40]
Open stub resonator	**Urine**	**1.25**	**66-74**	**2.53**	**Proposed**

Chapter 7

Conclusions

This thesis presented a new and improved sensing technology for different samples using microwave technology on the interaction between the substance under test (MUT) and the microwave electric field. This interaction is discussed in detail because designing new sensors requires a perfect understanding of sample echoes for microwave radiation. In this range, new types of resonators are designed and manufactured to obtain high sensitivity and high efficiency, which are fundamental in materials characterization.

7.1 Conclusions of Chapter 3

In this chapter, a new study relying on the negative electrical permittivity band to extract the electrical parameters of the equivalent circuit of complementary split ring resonators (CSRRs) loaded transmission line is proposed. CSRR coupled to microstrip transmission line has been suggested and the behavior of related frequency band of negative permittivity has been investigated, in order to provide the frequencies that are adopted in the calculation of electrical parameters of the equivalent circuit. The equivalent circuit has been simulated and a good agreement between the results obtained for resonant frequency derived from the simulation results and equivalent circuit model is obtained. Simulation results of transmission frequency rejection band remain compatible with results of equivalent circuit model when different lengths of transmission line are applied and hence, further validity of equivalent circuit is confirmed. The increment in host line capacitance, C leads to an increase of C_c value, hence shifting the interval of negative permittivity band to lower frequencies. This confirms that equivalent circuit parameters are influencing the negative permittivity.

7.2 Conclusions of Chapter 4

In this chapter, a new model of microwave planar sensor established on the complementary split ring resonator (CSRR) as well as an air hole in substrate of the structure is introduced for a precise measurement of materials permittivity. The CSRR is etched in the ground plane, while the hole is filled into substrate of the planar microstrip line. Two CSRRs structures with and without hole are selected for the sensitivity analysis, where the final is establish to hold over quite sensitivity and thus evidence to be more suitable for the sensor layout. The minimum transmission frequencies for each structure are observed relied on the permittivity of the specimen. A sensor in the form of CSRRs operating at a 1.74–3.4 GHz band is explained. At resonance, it is found that the electric field produced straight the plane of CSRR being highly sensitive for the characterization of sample resident with the sensor. The minimum transmission frequency of sensor shifts from 3.4 to 1.74 GHz as the sample permittivity varies from 1 to 10. A numerical model is introduced here for the computation of the system resolution as a function of resonance frequency and sample permittivity using electromagnetic simulator. the proposed sensor provides sensitivity between 1.2-2.5 times greater than sensitivity of conventional planer sensors have the same relative permittivity of the substrate (without hole).While, proposed sensor sensitivity reach to 3 times greater than conventional planer sensors have low loss Rogers substrate (without hole)

7.3 Coclusions of Chapter 5

In this chapter, we present a modified SRRs planar sensor for noninvasive, accurate complex permittivity measurements of solid dielectrics. Starting from the classical SRR, a modified structure, using vertical strips added at a close distance of 0.2 mm to the SRR is investigated both from the enhanced selectivity perspective and from the overall dimensions. The result is a sensor made of two modified SRRs with lateral vertical strips, exhibiting high sensitivity for two resonant frequencies, at 1.24 GHz and 2.08 GHz.

A simplified equivalent circuit model is used to explain the microwave sensor's design, and a very good agreement between the circuit model and the full electromagnetic simulation results is achieved. After a careful investigation, the two VS-SRRs sensor is selected to be further investigated For each resonant frequency, we consider the data obtained after full wave electromagnetic simulation and using a curve fitting tool, we determine analytical expressions for both the real and imaginary parts of the permittivity. These are expressed as a function of the resonant frequencies, the MUT's thickness, and the quality factor of the loaded sensor.

The sensor is implemented on an a ordable, commercial substrate, FR-4 substrate, with a thickness of 1.6 mm, with reduced dimensions and being able to measure the real and imaginary parts of the permittivity for di erent solid dielectric

samples, with errors less than 4.5% for both resonant frequencies in all analyzed cases. In our work, we have considered a large range of amples, with different thicknesses, different loss tangents, and dielectric constants to better vestigate the sensor's capabilities in real-life scenarios. The iversity of the samples helped us to observe the limitations of the numerical model developed in Section 5.2 and find solutions to overcome them, such as successfully using the second resonant frequency.

Also, we have measured the quality factor both for the unloaded and loaded sensor using the resonant frequency and the relative 3dB bandwidth of the resonator's frequency esponse.This approach added more practical consistency to our investigation. Still, some improvements can be done with respect to further miniaturization and the possibility to use this sensor for liquid dielectric characterization.

7.4   Conclusions of Chapter 6

A highly sensitive differential microstrip sensor for biomedical sensing applications is designed, fabricated, and tested. It consists of two identical parts, each of them made of a Wilkinson power divider and a transmission line loaded with two open-stub resonators. The structure is easily fabricated on a single metal microstrip layer. The Teflon beaker is placed on top of the microstrip surface instead of having a microfluid channel etched, thus simplifying the production process. The samples used for measurements were a mixture between water and urine with different percentages. The results were used to determine the complex permittivity of the liquid mixtures, including pure water and pure urine. Due to starting with different mixture sample that are supplied in the simulation, the data range of water content that was used in the simulation was recalibrated to match the same data range of the measured samples. As the result, good assent between the measured complex permittivity values and that forecasted by the Weiner model that extracted relying on simulation results. The values for the complex permittivity show good agreement with reference values. Additionally, the sensitivity of the sensor determined based on measurements is very good in comparison with similar works. The sensor can successfully be used in medical applications that require investigating the electrical parameters of urine in different medical conditions.

7.5   List of Original Contributions

- A new approach for extracting electrical parameters of the equivalent circuit of complimentary split ring resonators (CSRRs) loaded transmission line, based on the frequency band where negative electrical permittivity occurs, was proposed.   The procedure provides the electrical characteristics of CSRR (inductance, Lc, capacitance, Cc and intrinsic resonant frequencies). The obtained equivalent circuit model of CSRR loaded transmission line has been simulated and a good agreement is achieved between the results derived from the simulation and the ones form the equivalent circuit model. Further validity of the usage circuit is confirmed by applying different lengths of transmission line (host line). Nevertheless, the results of minimum insertion loss which were determined by the provided equivalent circuit model (which are proposed by the approach) are remaining compatible with the simulation. The results have been disseminated by publishing the paper [7.6,3].

- A new model of microwave planar sensor established on the complementary split ring resonator (CSRR) as well as an air hole in substrate of the structure is introduced for a precise measurement of materials permittivity. The CSRR structure with hole was selected for the sensitivity analysis, the result is established to hold over quite sensitive compared with CSRR structure without hole and thus evidence to be more suitable for the sensor design. A numerical paradigm was introduced for the computation of the system resolution as a assignment of resonance frequency and sample permittivity using electromagnetic simulator. The results can be noticed in my published paper [7.6,1].

- A sensor using modified Split Ring Resonators (SRRs) is designed, simulated, fabricated, and used for advanced investigation and precise measurements of the real part and imaginary part solid dielectrics' permittivity. The numerical simulations were used to develop a mathematical model based on a curve fitting tool for both resonant frequencies, allowing to obtain analytical relations for real and imaginary parts of permittivity as a function of the sample's thickness and quality factor. The sensor is designed and fabricated on 1.6 mm thick FR-4 substrate. The measurements of different samples, such as transparent glass, acrylic glass, plexiglass, and Teflon, confirm that the modified SRR sensor is easy to implement and gives accurate results for all cases, with measurement errors smaller than 4.5%. The results have been illustrated in my published paper [7.6,4].

- A microstrip highly sensitive differential sensor for complex permittivity characterization of urine samples is designed, fabricated, and tested. The sensor was easily implemented on an affordable substrate FR-4 Epoxy with a thickness of 1.6 mm. Different ratios of water-urine mixtures have been considered for measurement. Different samples of water content in urine were tested with percentages, such as 0% urine (100% water), 20% urine, 33% urine, 50% urine, 66% urine and 100% urine. The complex permittivity of the samples has been determined based on a mathematical model and the results of the measurements. The results have been represented in my published paper [7.6,5].

7.6   List of publications

1. A. A. Al-behadili, T. Petrescu, and I. A. Mocanu. "Complimentary Split Ring Resonator Sensor with High Sensitivity Based on Material Characterization." Telkomnika 18, no. 1 (2020): 272-281.

2. A. A. Al-behadili, and T. Petrescu. "Determination of Transmission Zero Frequency for Complementary Split-Ring Resonator/Split-Ring Resonator Unit Cells from Effective Permittivity and Permeability." In 2019 11th International Symposium on Advanced Topics in Electrical Engineering (ATEE), pp. 1-6. IEEE, 2019.

3. A. A. Al-behadili, T. Petrescu, and I. A. Mocanu. "Method of Extracting The Equivalent Circuit of Complementary Split Ring Resonator Loaded Transmission Line Relying on Negative Permittivity Characteristic." Revue Roumaine des Sciences Techniques-Serie Electrotechnique et Energetique 65, no. 1-2 (2020): 81-85.

4. A. A. Al-behadili, I. A. Mocanu, N. Codreanu, and M. Pantazica. "Modified split ring resonators sensor for accurate complex permittivity measurements of solid dielectrics." Sensors 20, no. 23 (2020): 6855.

5. A. A. Al-behadili, I. A. Mocanu, T. M. Petrescu and T. A. Elwi. " Differential Microstrip Sensor for Complex Permittivity Characterization of Organic Fluid Mixtures." Sensors, 21 (7865), pp. 2-20,2021. Doi.org/10.3390/s21237865.

7.7 Future Work

The ability to develop the approaches proposed is relying to the conclusions drawn In this thesis. Several future works could be offered to increase the current works' sensitivity, accuracy, and performance. Some recommendations and ideas for further work are follows:

In chapter five, the sensitivity of the sensor can be increased by raising the quality factor of the resonator VS-SRR. This is can be achieved by replacing high loss FR4 supstrate with low loss supstrate such as, Rogers RT/duroid 5870(tm), Rogers RT/duroid 5880(tm) etc.

In chapter six, the performance of the sensor can be improved by increasing wall height of the beaker, hence increase sample volume to enable more detailed evaluation of the liquid material properties. Moreover, a second teflon beaker could be put on the free two residual elements of an open stub of the sensor as shown in Figure 7.1, in order to used to compare characterize liquid dielectric samples such as detecting deficiency and impurity in the test liquid, when compearing with the reference, or can be used to characterize liquid samples improving the robustness to ecological factors producing cross-sensitivity or misstandarization.
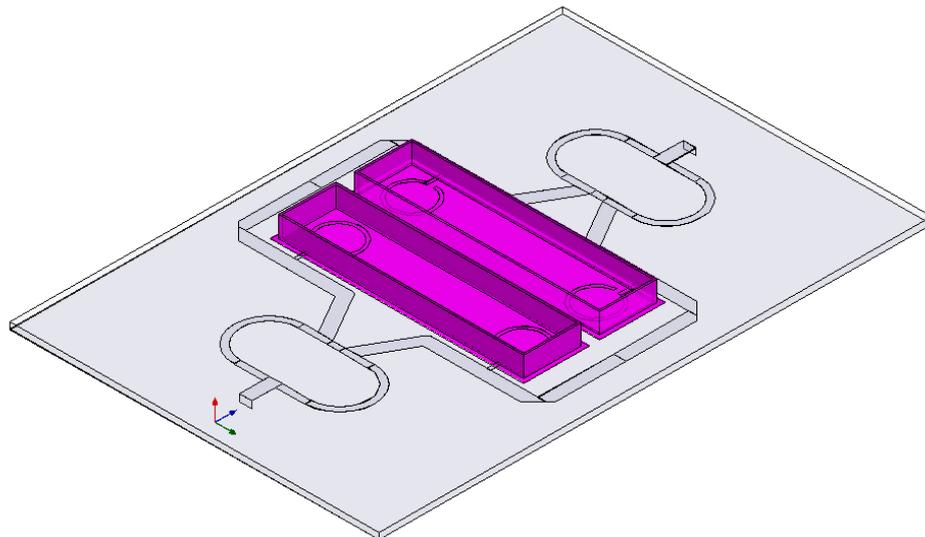

Figure 7.1   *The proposed sensor with two beakers for liquids testing applications.*

Despite quite accurate measurments were obtained from the proposed sensor in chapter six. However, the technique did not take into consideration the air gap between the sensor and the beaker-surface which is much important for the precise measurement of complex permittivity.

In order to solve this dilemma, a new study is proposed based on utillizing an external light-dependent resistor, LDR, or photo-conductive cell that connects to the sensor structure part which has direct influence on the insertion loss value of the sensor resonance frequency. The value of LDR changes according to the change of incident light on it, hence the value of insertion loss will influenced according to that. The operation system is intended to put the beaker holding the liquid sample above the surface of LDR, so the light coming from the beaker will change the value of the LDR, as shown in Figure 7.2 (a), (b).
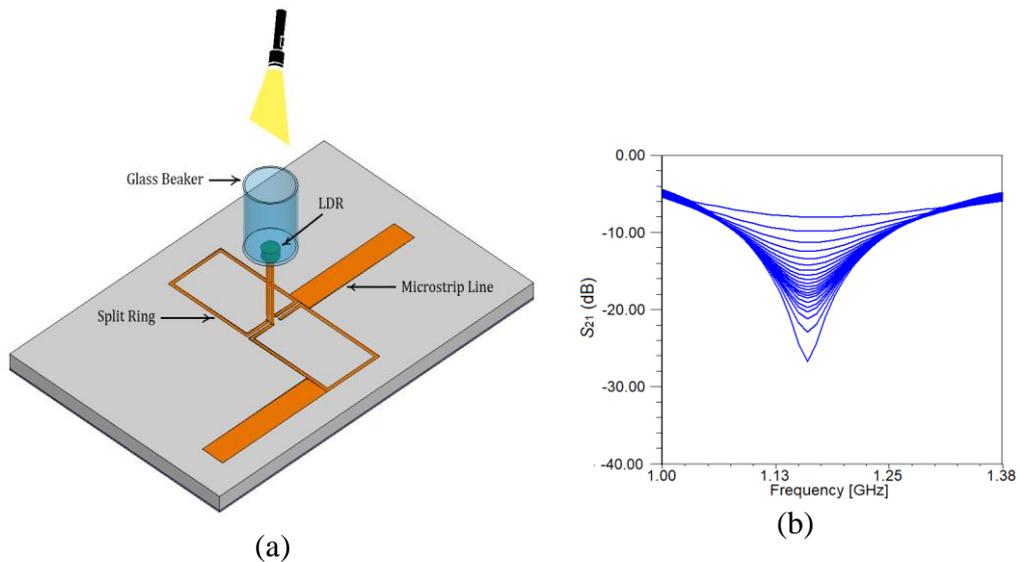

(a)

(b)

Figure 7.2 *(a) The proposed sensor based LDR for liquids testing applications, (b) transmission response of the liquid sample when changes from high concentration to low concentration detected by variation in intensity of incident light on LDR surface.*

It is clear from the above, that the sensor performance depends entirely on the quality standard of LDR sensitivity, hence the limitation imposed by the air gap that accompanies most of the microstrip sensor techniques is completely eliminated.

Bibliography

[1] A.A. Abduljabar, *Compact microwave microfluidic sensors and applicator*, PhD diss., Cardiff University, 2016.

[2] Y. Zhao, Y. Li, B. Pan, S.H. Kim, Z. Liu, M.M. Tentzeris, J. Papapolymerou, M. G. Allen, *RF evanescent-mode cavity resonator for passive wireless sensor applications*, Sensors and Actuators A: Physical, 161(1-2), pp. 322-328, 2010.

[3] C. Elbuken, T. Glawdel, D. Chan, C.L. Ren, *Detection of microdroplet size and speed using capacitive sensors*, Sensors and Actuators A: Physical, 171(2), pp. 55-62, 2011.

[4] L.F. Chen, C.K. Ong, C.P. Neo, V.V. Varadan, V.K. Varadan, *Microwave electronics material measurements and characterization*, John Wiley and Sons, Ltd, 2004.

 [5] A. technologies, *Basics of measuring the dielectric properties of materials*, Agilent technologies Application Note, 2006.

[6] Alahnomi, A. Rammah, Z. Zakaria, E. Ruslan, A.A. Bahar, *A novel symmetrical split ring resonator based on microstrip for microwave sensors*, Measurement Science Review, 16(1), pp. 21-27, 2016.

[7] Khan, M.T., Ali, S.M, *A brief review of measuring techniques for characterization of dielectric materials*, Int. J. Inf. Technol. Electr. Eng., 1(1), pp. 1-5, 2012

[8] Venkatesh, M.S., Raghavan, G.S.V, *An overview of dielectric properties measuring techniques*, Can. Biosyst. Eng., 47(7), pp. 15-30, 2005

[9] Jha, S.N., Narsaiah, K., Basediya, A.L., Sharma, R., Jaiswal, P., Kumar, R., Bhardwaj, R, *easurement techniques and application of electrical properties for nondestructive quality evaluation of foods—Areview*, Journal of Food Sci. Technol., 48(4), pp. 387-411, 2011.

[10] Alahnomi, A. Rammah, et al., *Review of Recent Microwave Planar Resonator-Based Sensors: Techniques of Complex Permittivity Extraction, Applications, Open Challenges and Future Research Directions*, Sensors, 21(7), pp. 2267, 2021.

[11] Ansari, M.A. Hussain, A.K. Jha, M.J. Akhtar, *Design and Application of the CSRR Based Planar Sensor for Non-Invasive Measurement of Complex Permittivity*, IEEE Sens. J., 15(12), pp. 7181-7189, 2015.

[12] S. Kayal, T. Shaw, D. Mitra, *Design of Metamaterial-Based Compact and Highly Sensitive Microwave Liquid Sensor*, Appl. Phys. A Mater. Sci. Process., 126(1), pp. 1-9,2020.

[13] E.L. Chuma, Y. Iano, G. Fontgalland, L.L Bravo Roger,. *Microwave Sensor for Liquid Dielectric Characterization Based on Metamaterial Complementary Split Ring Resonator*, IEEE Sens. J., 18(24), pp. 9978-9983, 2018. [CrossRef]

[14] W. Withayachumnankul, K. Jaruwongrungsee, A. Tuantranont, C. Fumeaux, D. Abbott, *Metamaterial-Based Microfluidic Sensor for Dielectric Characterization*, Sens. Actuators A Phys., 189, pp. 233-237,2013. [CrossRef]

[15] J. Rivera, M. Carrillo, M. Chacón, G. Herrera, G. Bojorquez, *Self-calibration and optimal response in intelligent sensors design based on artificial neural networks*, Sensors, 7(8), pp. 1509-1529, 2007. [CrossRef]

[16] I. J. Bahl, *Lumped Elements for RF and Microwave Circuits*, Artech House microwave library, pp. 24-27, 2003.

 [17] M. D. Pozar, *Microwave engineering*, 4th edition, John Wiley & Sons, pp.177-193, 2012.

[18] J. Bonache, M. Gil, I. Gil, J. García-García, F. Martín, *On the electrical characteristics of complementary metamaterial resonators*, IEEE Microwave. Wireless Compon. Lett., 16(10), pp. 543–545, 2006.

[19] J. Bonache, M. Gil, I. Gil, J. Garcia-Garcia, F. Martin, *On the electrical characteristics of complementary metamaterial resonators*, IEEE Microwave and Wireless Components Letters, 16(10), pp. 543-545, Oct. 2006.

[20] M. S. Boybay, O. M. Ramahi, *Material Characterization Using Complementary Split-Ring Resonators*, in IEEE Transactions on Instrumentation and Measurement, 61(11), pp. 3039-3046, Nov. 2012.

[21] J.B. Pendry, A.J. Holden, D.J. Robbins, W.J. Stewart, *Magnetism from conductors and enhanced nonlinear phenomena*. IEEE Trans. Microw. Theory Tech., 47(11), pp. 2075-2084, 1999.

[22] G. Galindo-Romera,; F.J. Herraiz-Martínez, M. Gil, J.J. Martinez-Martinez, Segovia-argas, *Submersible Printed Split-Ring Resonator-Based Sensor for Thin-Film Detection and Permittivity Characterization*, IEEE Sens. J., 16(10), pp. 3587-3596, 2016.

[23] C.-S. Lee, C.-L. Yang, *Complementary split-ring resonators for measuring dielectric constants and loss tangents*. IEEE Microw. Wireless Compon. Lett., 24(8), pp. 563-565, 2014. [CrossRef]

 [24] Rhode, Schwarz, *Measurement of Dielectric Material Properties Application Note*, Availableonline:https://cdn.rohde-chwarz.com/pws/dl_downloads/dl_application/00aps_undefined/RAC-0607-0019-1-5E.pdf (accessed on 20 September 2020).

[25] Physical Properties of Acrylic Sheets. Available online: https://www.builditsolar.com/ References/Glazing/ physicalpropertiesAcrylic.pdf (accessed on 20 September 2020).

[26] A.K. Verma, A.S. Omar, *Microstrip resonator sensors for determination of complex permittivity of materials in sheet, liquid and paste forms*. Microw. Antennas Propag. IEE Proc., 152(1), pp. 47-54, 2005. [CrossRef]

[27] A. L. Mckenzie, L. E. Armstrong, *Monitoring Body Water Balance in Pregnant and Nursing Women: The Validity of Urine Color*, Annalas of Nutrition and Metabolism, 70 (l1),pp. 18-22, 2017.

[28] L. E. Armstrong, M. S. Ganio, J. F. Klau, E. C. Johnson, D. J. Casa, C. M. Maresh, *Novel hydration assessment techniques employing thirst and a water intake challenge in healthy men*, Applied physiology, Nutrition, and Metabolism,. 39(2), pp. 138-144, 2013.

[29] A. Al-Fraihat, A. Wesam Al-Mufti, U. Hashim, T. Adam, *Potential of urine dielectric properties in classification of stages of breast carcinomas*, 2nd International Conference on Electronic Design (ICED), 2014, pp. 305-308, doi: 10.1109/ICED.2014.7015819.

[30] G. M. Rocco, M. Bozzi, D. Schreurs, L. Perregrini, S. Marconi, G. Alaimo, F. Auricchio, *3-D Printed Microfluidic Sensor in SIW Technology for Liquids' Characterization*, IEEE Transactions on Microwave Theory and Techniques, 68(3), pp. 1175-1184, March 2020, doi: 10.1109/TMTT.2019.2953580.

[31] E. L. Chuma, Y. Iano, G. Fontgalland, L. L. Bravo Roger, *Microwave Sensor for Liquid Dielectric Characterization Based on Metamaterial Complementary Split Ring Resonator*, IEEE Sensors Journal, 18(24), pp. 9978-9983, 15 Dec.15, 2018, doi: 10.1109/JSEN.2018.2872859.

[32] A. Ebrahimi, J. Scott, K. Ghorbani, *Ultrahigh-Sensitivity Microwave Sensor for Microfluidic Complex Permittivity Meas-urement*, IEEE Transactions on Microwave Theory and Techniques, 67(10), pp. 4269-4277, Oct. 2019, doi: 10.1109/TMTT.2019.2932737.

[33] P. Velez, L. Su, K. Grenier, J. Mata-Contreras, D. Dubuc, F. Martin, *Microwave microfluidic sensor based on a microstrip splitter/combiner configuration and split ring resonators (SRRs) for dielectric characterization of liquids*, IEEE Sensors J., 17(20), pp. 6589-6598, Oct. 2017.

[34] P. Vélez, K. Grenier, J. Mata-Contreras, D. Dubuc, F. Martín, *Highly-Sensitive Microwave Sensors Based on Open Com-plementary Split Ring Resonators (OCSRRs) for Dielectric Characterization and Solute Concentration Measurement in Liquids*, IEEE Access, 6, pp. 48324-48338, 2018, doi: 10.1109/ACCESS.2018.2867077.

[35] C.-H Li, K. Chen, C. Yang, C. Lin K. Hsieh, *A urine testing chip based on the complementary split-ring resonator and mi-crofluidic channel*, IEEE Micro Electro Mechanical Systems (MEMS), 2018, pp. 1150-1153, doi: 10.1109/MEMSYS.2018.8346765.

[36] P. Vélez, J. Muñoz-Enano, M. Gil, J. Mata-Contreras, F. Martín, *Differential Microfluidic Sensors Based on Dumbbell-Shaped Defect Ground Structures in Microstrip Technology: Analysis, Optimization, and Applications*, Sensors, 19, 3189, 2019, doi:10.3390/s19143189.

[37] H.-Y. Gan et al., *Differential Microwave Microfluidic Sensor Based on Microstrip Complementary Split-Ring Resonator (MCSRR) Structure*, IEEE Sensors Journal, 20,(11), pp. 5876-5884, 1 June1, 2020, doi: 10.1109/JSEN.2020.2973196.

[38] A. Ebrahimi, F.J. Tovar-Lopez, J. Scott, K. Ghorbani, *Differential microwave sensor for characterization of glycerol–water solutions*, Sensors Actuators B Chem., 321, 128561, 2020, doi:10.1016/j.snb.2020.128561.

[39] J. Muñoz-Enano, P. Vélez, M. Gil, F. Martín, *Microfluidic reflective-mode differential sensor based on open split ring reso-nators (OSRRs)*, Int. J. Microw. Wirel. Technol., 12, pp. 588–597, 2020, doi:10.1017/s1759078720000501.

[40] B.-X. Wang, W.-S. Zhao, D.-W. Wang, W.-J. Wu, Q. Liu, G. Wang, *Sensitivity optimization of differential microwave sensors for microfluidic applications*, Sensors Actuators A Phys., 330, 112866, 2021, doi:10.1016/j.sna.2021.112866.